JOURNAL OF MATERIALS SCIENCE 23 (1988) 3997–4003

$SrTiO_3$ glass ceramics

Part I *Crystallization and microstructure*

S. L. SWARTZ
Battelle Columbus Division, Columbus, Ohio, USA

E. BREVAL
Materials Research Laboratory, Pennsylvania State University, University Park, Pennsylvania, USA

C. A. RANDALL
University of Essex, Colchester, UK

B. H. FOX
Ontario Research Foundation Toronto, Ontario, Canada, USA

This is the first in a series of two papers describing the crystallization and dielectric properties of glass-ceramics derived from a particular strontium titanium aluminosilicate glass composition. This first paper concerns the development of crystalline phases and microstructure of glass–ceramics prepared under various crystallization conditions. In the following paper, the dielectric properties of these glass–ceramics are described and correlated with the characterization results.

Perovskite strontium titanate ($SrTiO_3$) was the primary crystalline phase in glass–ceramics crystallized over the temperature range of 800 to 1100° C. At crystallization temperatures below 950° C, $SrTiO_3$ formed with a spherulitic or dendritic growth habit. X-ray diffraction suggested that the $SrTiO_3$ crystallized in a perovskite-like "precursor" phase which transformed to perovskite $SrTiO_3$ with further crystallization time. However, electron diffraction indicated that this "precursor" phase was cubic perovskite $SrTiO_3$. At higher crystallization temperatures, perovskite $SrTiO_3$ was present as individual crystallites without evidence of the spherulitic habit. The crystallization of $SrTiO_3$ was followed by that of other phases, the hexacelsian and anorthite forms of $SrAl_2Si_2O_8$, and the rutile and anatase forms of TiO_2. The crystallization sequence and microstructure of the glass–ceramics were determined by the competition for strontium and titanium between the crystallizing phases, $SrTiO_3$ and $SrAl_2Si_2O_8$, and TiO_2.

1. Introduction

Several studies into the crystallization of glass–ceramics containing ferroelectric perovskite phases have been reported. Specifically, both the $BaTiO_3$ [1–3] and the $PbTiO_3$ [4–6] glass–ceramic systems have received considerable attention. These studies have demonstrated the importance of the relationship between microstructure and dielectric properties of glass–ceramics. No detailed investigation into the crystallization and dielectric properties of $SrTiO_3$ glass–ceramics has appeared in the literature, although these materials have been studied with respect to several low temperature applications, such as cryogenic temperature sensors [7–8].

A microstructural study has been performed on $SrTiO_3$ containing glass–ceramics, as part of a larger investigation into their dielectric properties [9]. Glass–ceramics were prepared from a glass of a particular SrO–TiO_2–SiO_2–Al_2O_3 composition by crystallization over a wide range of temperature and time. The crystalline phases that occurred with the various crystallization conditions were identified by X-ray diffraction, and the resulting glass–ceramic microstructures were examined by scanning and transmission electron microscopy. In this paper, the results of this crystallization study will be described.

2. Glass composition and crystallization

The glass–ceramics were derived from a glass with nominal composition: 65 wt % of $SrTiO_3$ and 35% of SiO_2 and Al_2O_3. The amounts of SiO_2 and Al_2O_3 were such that the weight ratio of the silica to alumina was 2 : 1. Other glass compositions were investigated, and it was found that the crystallization behaviour was sensitive to factors such as the silica–alumina ratio and the amount of $SrTiO_3$ in the parent glass [9–10]. In this paper, only the results of this particular glass composition will be reported.

The glass was melted in platinum crucibles at 1650° C for 2 h. The molten glass was poured into copper moulds, so that glass slabs of 10 × 5 × 1 cm were obtained; the glass was then annealed at 760° C

0022–2461/88 $03.00 + .12

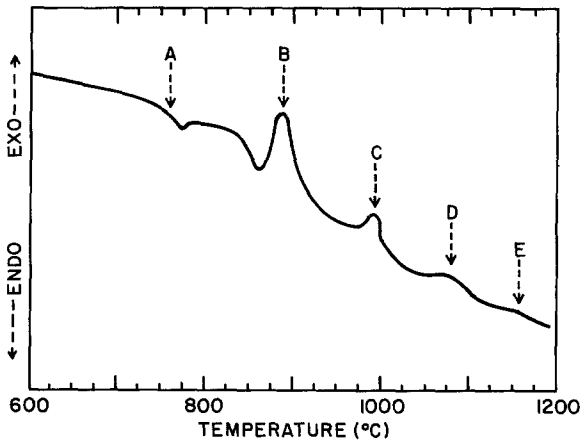

Figure 1 A typical DTA trace. (A annealing point, B $SrTiO_3$, C $SrAl_2Si_2O_8$ (hexacelsian), D TiO_2 (anatase), E $SrAl_2Si_2O_8$ (anorthite)).

for 17 h. Chemical analyses of the glass were performed, and this information appears in Table I; the glass composition is given in both weight and mole per cent, with trace element concentrations given in parts per million. These data verified that the final glass composition was close to that of the batched composition, and that no appreciable amount of impurities were introduced during the melting operation.

Samples for the crystallization studies were cut from the glass slabs by sectioning with a diamond saw and core drilling discs, 9 mm in diameter by 1 mm thick, with an ultrasonic cutting tool. The presence of reduced titanium (Ti^{3+}), caused by the incorporation of hydroxyl ions during melting, was indicated from dielectric measurements of as-annealed glass [9]. For this reason, prior to crystallization, glass samples were subjected to a heat treatment at 700° C for 100 h, to re-oxidize the Ti^{3+}; this heat treatment schedule was determined from the results of an earlier study [11]. A brown to clear colouration change in the glass samples was observed with this heat treatment, consistent with the results of earlier work [11].

Crystallization of the glass was studied by DTA, and by X-ray diffraction, TEM, and SEM of crystallized glass–ceramic samples. Crystallization conditions were isothermal; glass samples were immersed in a furnace at temperatures from 800 to 1100° C, and removed after various times (0.25 to 64 h). With crystallization temperatures of 800 and 850° C, crystallization occurred somewhat slowly, as evidenced by a colouration change from clear to opaque white. The onset of crystallization as determined by this colouration change occurred after four hours at 800° C, 20 min at 850° C, and almost immediately at higher temperatures.

TABLE I Chemical analyses of SrO–TiO_2–Al_2O_3–SiO_2 glass

	Wt %	Mol %	Impurities (p.p.m.)	
SrO	37.9	30.4	B	30
TiO_2	26.6	27.7	Ta	< 100
SiO_2	23.1	31.8	Fe	20
Al_2O_3	12.4	10.1	Zr	< 10
			Ba	100
			Ca	50

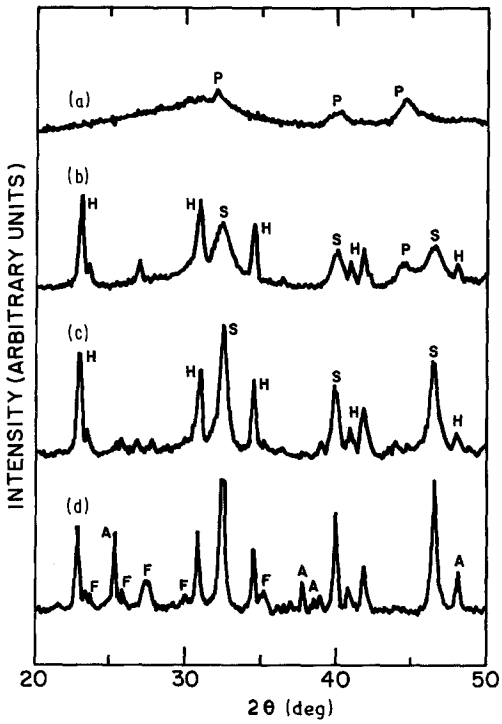

Figure 2 X-ray diffraction data for glass–ceramics crystallized for 1 h at (a) 850° C, (b) 900° C, (c) 1000° C and (d) 1100° C.

3. Results

3.1. Differential thermal analysis

Differential thermal analysis (DTA) scans were run with a Perkin–Elmer thermal analysis system from room temperature to 1200° C with a heating rate of 10° C min^{-1}. A typical DTA trace is presented in Fig. 1. An endothermic peak was observed at 780° C, due to the glass transition. Two large exothermic peaks were observed at about 890 and 980° C. Later X-ray diffraction studies confirmed that the exothermic peak at 890° C was due to the crystallization of perovskite $SrTiO_3$, and the exothermic peak at 980° C corresponded to the crystallization of hexacelsian $SrAl_2Si_2O_8$. Two minor peaks were observed at 1070 and 1160° C; X-ray diffraction suggested that these peaks corresponded to the crystallization of anatase TiO_2 and the transformation of the $SrAl_2Si_2O_8$ phase from hexacelsian to anorthite.

3.2. X-ray diffraction

Crystalline phases were identified by the use of a Phillips APD-3600 automated X-ray diffraction system. XRD scans were taken on powdered glass–ceramic samples for 2θ at a rate of approximately 2° min^{-1} (CuKα radiation). The phase progression in these glass–ceramics with crystallization temperature and time, derived from the XRD data, is summarized in Table II. X-ray diffraction data are presented as a series of XRD patterns of glass–ceramics given 1 h crystallizations at temperatures of 850, 900, 1000, and 1100° C, in Fig. 2.

At low crystallization temperatures (< 950° C), XRD data suggested that perovskite $SrTiO_3$ did not crystallize directly from the glass, but formed via a "precursor" phase, with a structure slightly different from perovskite. It was impossible to determine the exact structure of this precursor phase from the XRD

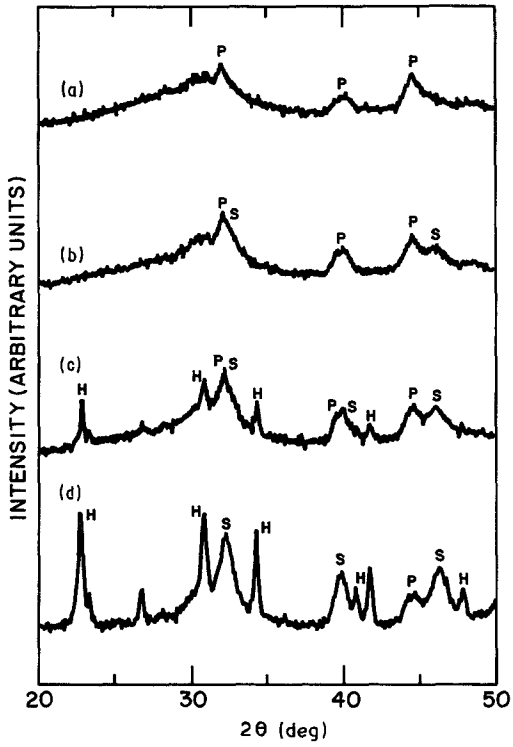

Figure 3 XRD patterns of glass–ceramics crystallized at 850° C for (a) 1 h (b) 4 h (c) 16 h and (d) 64 h.

data, because of line broadening due to fine crystallite size. The *d*-spacings corresponding to the precursor phase (0.281, 0.225, 0.204, 0.190, and 0.162 nm) were close to those of perovskite $SrTiO_3$ (0.276, 0.225, 0.195, and 0.159 nm). Most of the major perovskite peaks appeared in the XRD patterns, although they were shifted somewhat in position and intensity. However, in these XRD patterns, a major peak was observed at 0.204 nm, which could not be attributed to perovskite $SrTiO_3$.

The precursor phase first appeared after 4 h at 800° C, 20 min at 850° C, and almost immediately at 900° C, consistent with the visual observations of the clear to opaque white colouration change. The transformation of the precursor phase to perovskite $SrTiO_3$ is shown by a series of XRD patterns of glass–ceramics crystallized at 850° C, in Fig. 3. With increasing crystallization time, the positions of XRD peaks shifted slightly, toward the *d*-spacings expected for perovskite $SrTiO_3$, and the anomalous peak at 0.204 nm decreased in intensity. At low crystallization temperatures (800 to 900° C), this apparent transformation was sluggish,

TABLE II Progression of crystalline phases occurring with crystallization temperature and time

800° C	precursor phase (X) → perovskite $SrTiO_3$
850° C	(X) → perovskite $SrTiO_3$ hexacelsian $SrAl_2Si_2O_8$ (after 16 h)
900° C	(X) → perovskite $SrTiO_3$ hexacelsian $SrAl_2Si_2O_8$ (after 30 min)
1000° C	perovskite $SrTiO_3$ $SrAl_2Si_2O_8$ (hexacelsian → trace anorthite) trace anatase TiO_2 (after 2 h)
1100° C	perovskite $SrTiO_3$ $SrAl_2Si_2O_8$ (hexacelsian → anorthite) TiO_2 (anatase → trace rutile)

as the XRD peak at 0.204 nm was present, even after the longest crystallization times investigated. This peak was also observed with low intensity in the XRD patterns of glass–ceramics crystallized at 950° C for 1 h and up to 30 min at 1000° C, although the perovskite $SrTiO_3$ phase was well established in these glass–ceramics. With higher crystallization temperatures (1000 to 1100° C), the crystallization of perovskite $SrTiO_3$ was rapid, and the amount of $SrTiO_3$ in the glass–ceramics did not appear to increase appreciably with crystallization time. Quantitative XRD analysis was inconclusive because of the large differences in XRD peak profiles and the presence of a significant amount of residual glass in the glass–ceramics.

Estimates of the $SrTiO_3$ crystallite sizes by XRD line broadening were made using the Scherer equation [12]. This method was not conclusive for the study of these glass–ceramics because of several complicating factors: (1) the coexistence of the precursor and perovskite $SrTiO_3$ phases; (2) a large proportion of residual glass at low crystallization temperatures; and (3) the effect of strain on the $SrTiO_3$ crystallites due to clamping by the glass–ceramic matrix [6]. Nonetheless, XRD line broadening indicated $SrTiO_3$ crystallite sizes of less than 20 nm for glass–ceramics crystallized below 1000° C, increasing to about 30 nm in glass–ceramics crystallized at 1000° C. The crystallite sizes increased slightly with crystallization time. Only minimal line broadening was observed in glass–ceramics crystallized at 1100° C, indicating a much larger crystallite size.

As the crystallization temperature was increased, the formation of $SrTiO_3$ was followed by that of other phases from the glass matrix. The first secondary phase to crystallize from the matrix was hexacelsian $SrAl_2Si_2O_8$; this phase first appeared after 16 h at 850° C, 30 min at 900° C, and almost immediately at higher temperatures. The XRD peaks corresponding to this phase were much narrower than those of $SrTiO_3$, indicating a larger crystallite size of the hexacelsian phase. Unlike the low temperature (< 950° C) crystallization of $SrTiO_3$, the crystallization of hexacelsian $SrAl_2Si_2O_8$ was complete after a relatively short time, as evidenced by the fact that once the hexacelsian phase was formed, XRD peak intensities were unaffected by a further increase of crystallization time.

The hexacelsian $SrAl_2Si_2O_8$ phase transformed to anorthite, a triclinic feldspar, at crystallization temperatures of 1000 and 1100° C. Traces of the anorthite phase were first detected in glass–ceramics crystallized for the longer times at 1000° C, and at 1050° C for 1 h. At 1100° C, the hexacelsian phase crystallized first, and was followed by the gradual transformation to anorthite; the transformation was complete after 8 h. The crystallization of titania also occurred at high crystallization temperatures. For crystallization times of greater than two hours at a temperature of 1000° C, a trace amount of anatase TiO_2 was detected. The amount of anatase increased for glass–ceramics crystallized at 1050 and 1100° C. In the glass–ceramics crystallized for longer times at 1100° C, some of the TiO_2 was present as rutile.

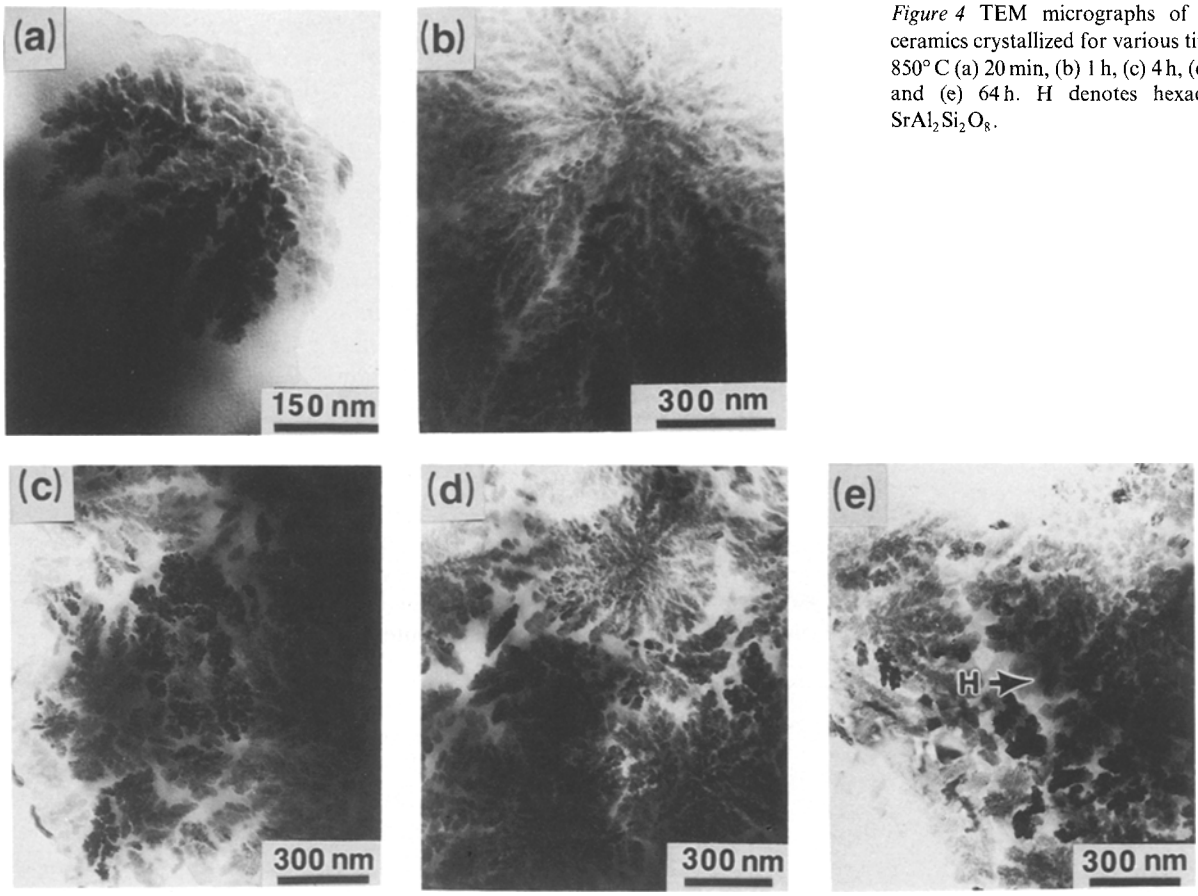

Figure 4 TEM micrographs of glass–ceramics crystallized for various times at 850° C (a) 20 min, (b) 1 h, (c) 4 h, (d) 16 h and (e) 64 h. H denotes hexacelsian $SrAl_2Si_2O_8$.

3.3. Microstructure

Microstructural and analytical techniques were applied to the glass–ceramics crystallized between 850 and 1100° C with a Phillips EM-420 TEM and a Joel 200-CX TEM, both of them fitted with energy dispersive spectrometers. The TEM samples were prepared by mechanical polishing of thin sections, followed by ion beam milling. Further microstructural information was obtained for glass–ceramics crystallized at 1100° C by scanning electron microscopy with an ISI DS-130 SEM equipped with KEVEX system 7000 EDS (energy dispersive spectroscopy). The SEM analysis was performed on glass–ceramic surfaces which were polished with cerium oxide and etched for 10 sec with a 5% solution of HF.

The microstructural development in the early stages of crystallization is shown by TEM data of glass–ceramics crystallized at 850° C, in Fig. 4. Initial crystallization at 850° C occurred after 20 min. The microstructure of this sample (Fig. 4a) consists of isolated spherulites of up to 0.5 μm in diameter, composed of radiating dendrites. These dendrites appeared to be composed of individual crystallites of about 20 nm in size. A selected area electron diffraction (SAED) pattern of one of these spherulites in the sample crystallized for 20 min at 850° C (Fig. 5), corresponds to a $\langle 0\,1\,0 \rangle$ zone axis diffraction pattern of perovskite $SrTiO_3$. The fine structural spot splitting of the reflections in this pattern was caused by misorientations within the $SrTiO_3$ crystal. These data indicate that the crystalline phase present during the early stages of crystallization was perovskite $SrTiO_3$, even though XRD data suggested a precursor phase with a slightly different structure. Continuous growth of the $SrTiO_3$ spherulites from the glassy matrix was observed with increasing crystallization time (1 and 4 h), as the microstructure became a network of interlocking dendritic crystals (Figs 4b and 4c). The hexacelsian $SrAl_2Si_2O_8$ phase was observed in glass–ceramics crystallized at 850° C for 16 and 64 h, in agreement with XRD results. The development of this phase is shown by the microstructure of these samples, in Figs 4d and 4e. The hexacelsian phase grew interstitially around the dendritic $SrTiO_3$ crystals, and was present as equiaxed crystals of about 50 nm in size.

TEM microstructures of glass–ceramics crystallized for 1 h at 900 and 1000° C are shown in Fig. 6. The development of the perovskite $SrTiO_3$ and hexacelsian $SrAl_2Si_2O_8$ phases proceeded differently than at lower temperatures. In the sample crystallized at 900° C for

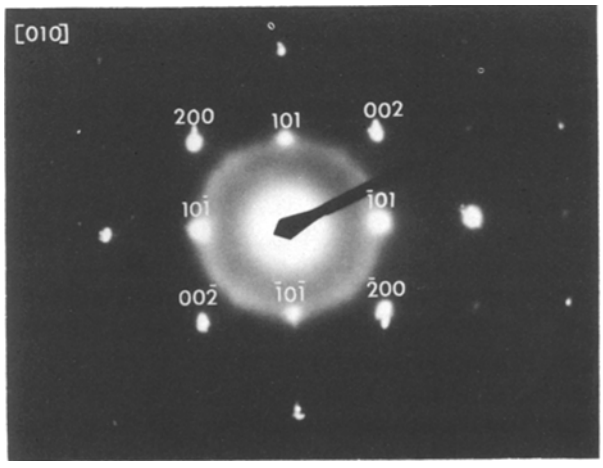

Figure 5 SAED pattern of dendritic crystal cluster from glass–ceramic crystallized at 850° C for 20 min.

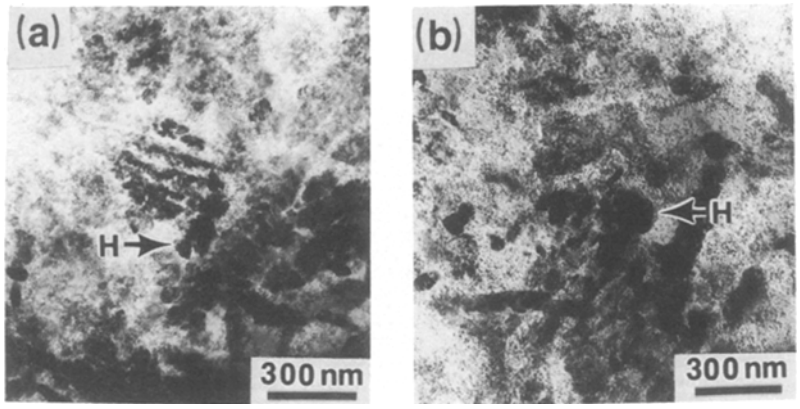

Figure 6 TEM micrographs of glass–ceramics crystallized for 1 h at (a) 900° C and (b) 1000° C.

1 h (Fig. 6a), dispersed crystallites of $SrTiO_3$ were observed, and the dendritic nature was almost completely absent. Also, oblong crystals (about 100 nm) of the hexacelsian phase were apparent. In the glass–ceramic crystallized at 1000° C for 1 h (Fig. 6b), a more pronounced dispersion of $SrTiO_3$ crystallites was observed. The hexacelsian crystals were larger in size and more oblong. The crystallite size of $SrTiO_3$ in glass–ceramics crystallized at 900 and 1000° C was less than 25 nm, in agreement with XRD data.

The microstructures of glass–ceramics crystallized at 1100° C were very different from those with lower crystallization temperatures, consistent with the XRD observation of multiple crystalline phases. SEM micrographs of glass–ceramics crystallized at 1100° C for 2, 4, and 8 h appear in Fig. 7. A dispersed phase of less than 1 μm (presumably $SrTiO_3$) was vaguely apparent in these micrographs; however, the most striking feature was the development of large, acicular crystals appearing after a crystallization time of 4 h. With further crystallization time, these acicular crystals increased in size, from up to 10 μm in length after 4 h to 80 μm in length after 16 h. An SEM micrograph of the 16 h sample appears in Fig. 8, along with a corresponding EDS-derived titanium map. Titanium was evenly distributed throughout the microstructure (corresponding to the dispersed $SrTiO_3$ phase). However, an increased density of titanium was observed in the regions of the acicular crystals, indicating that the acicular phase was titania.

Further microstructural information was obtained by TEM of the glass–ceramic crystallized at 1100° C for 4 h (Fig. 9). A TEM micrograph of an area between the acicular titania crystals appears in Fig. 9a. The $SrTiO_3$ crystals were much larger (500 nm) and displayed a faceted growth habit. The interstitial $SrAl_2Si_2O_8$ phase was identified by SAED as anorthite in this sample, in agreement with XRD data. Heavy "twinning" was also observed within the anorthite crystals. No evidence of the hexacelsian phase was found, although XRD suggested that at least some of the silicate phase was present in this form. Both the anatase and rutile forms of titania were observed, again as suggested by XRD. The acicular titania phase was identified as rutile, whereas the anatase was present in lesser quantity as smaller (200 nm), equiaxed crystals. A TEM micrograph of one of the acicular rutile crystals is shown in Fig. 9b. Crystallographic shear planes (a) and anti-phase boundaries (b) within the rutile crystal are indicated.

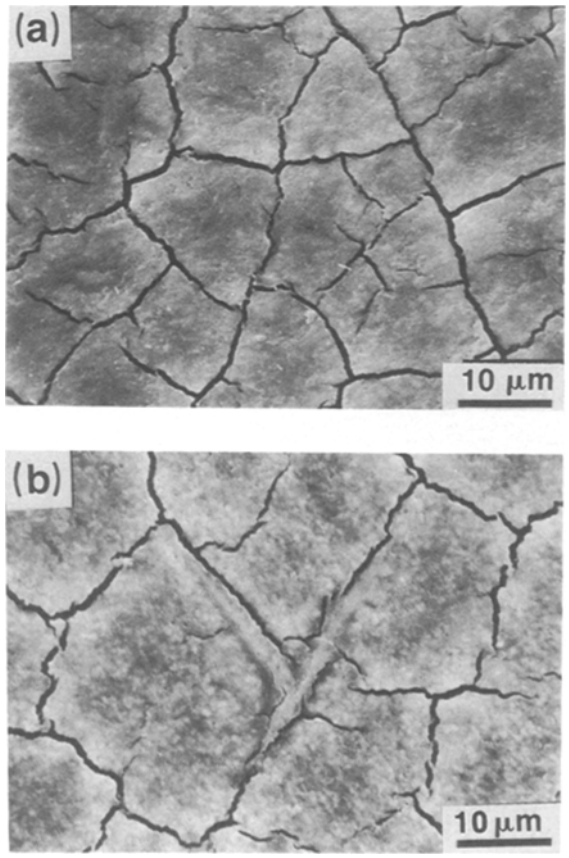

Figure 7 SEM micrographs of glass–ceramics crystallized at 1100° C for (a) 2 h, (b) 4 h and (c) 8 h.

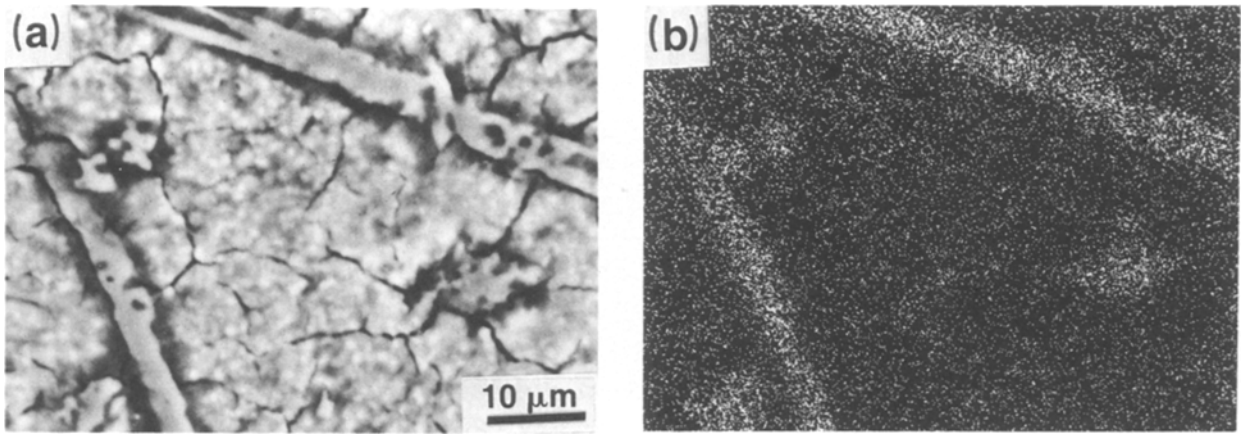

Figure 8 SEM micrograph and (b) corresponding EDS titanium map of glass–ceramic crystallized at 1100° C for 16 h.

4. Discussion

In the early stages of crystallization, the XRD patterns were difficult to interpret due to the extremely fine crystallite sizes in the glass–ceramics, preventing a non-ambiguous structural determination of the precursor phase by XRD. However, structural information obtained by TEM indicated that the precursor phase was perovskite $SrTiO_3$. Perhaps, the anomalous XRD data was a result of short-range ordering in the very initial stages of $SrTiO_3$ crystallization.

The complex crystallization sequence of these glass–ceramics can be summarized as follows: (1) the crystallization of perovskite $SrTiO_3$; (2) the crystallization of $SrAl_2Si_2O_8$ (as hexacelsian or anorthite); and (3) the crystallization of TiO_2 (as anatase or rutile). A competition for SrO existed between the $SrTiO_3$ and $SrAl_2Si_2O_8$ phases during crystallization of the glass–ceramic. The crystallization of $SrTiO_3$ could not be taken to completion before the crystallization of $SrAl_2Si_2O_8$ occurred, thereby decreasing the yield of $SrTiO_3$. This was likely caused by a depletion of SrO and TiO_2 in the region of the nucleating $SrTiO_3$ crystals. The residual glass in these depleted regions apparently was of a composition more conducive to the crystallization of $SrAl_2Si_2O_8$.

The appearance of titania in the glass–ceramics with the higher crystallization temperatures was not unexpected on the basis of the initial glass composition. The molar ratio of strontium to titanium was close to unity, so that excess TiO_2 would have been present in the residual glass after the crystallization of $SrTiO_3$ and $SrAl_2Si_2O_8$. The balance between the $SrTiO_3$ and $SrAl_2Si_2O_8$ phases determined the amount of TiO_2 available to crystallize. The glass composition also dictated that a residual glass existed after the crystallization of $SrTiO_3$, $SrAl_2Si_2O_8$, and TiO_2. The residual glass consisted of SiO_2 and Al_2O_3; its exact composition was determined by the relative amounts of the crystalline phases.

It is interesting to note that the hexacelsian $SrAl_2Si_2O_8$ is metastable at temperatures below its melting point of 1650° C [13], although the same hexacelsian phase has been observed in analogous $BaO–TiO_2–SiO_2–Al_2O_3$ glass–ceramics [1–2]. The densities of hexacelsian and anorthite are 2.99 and 3.17 $g\,cm^{-3}$, respectively. The crystallization of hexacelsian in preference to anorthite was likely related to the density of the residual glass prior to crystallization of hexacelsian. The density of uncrystallized glass was 3.20 $g\,cm^{-3}$; after crystallization of $SrTiO_3$ (5.12 $g\,cm^{-3}$), the density of the residual glass would be much lower. Since deformation or a significant density change during crystallization did not occur, stresses would have been exerted by the residual glass matrix on the $SrAl_2Si_2O_8$ crystals as they formed; these stresses would have favoured crystallization of

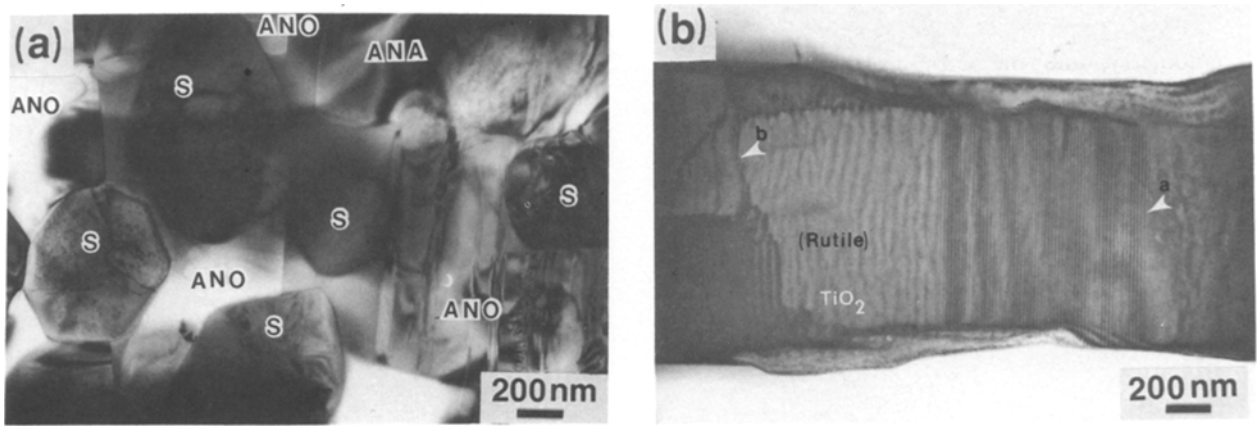

Figure 9 TEM micrographs taken on the glass–ceramic crystallized at 1100° C for 4 h (a) area showing $SrTiO_3$ (S), anorthite (ANO) and anatasr (ANA) crystal phases and (b) potion of acicular rutile crystal, showing crystallographic shear planes (A) and anti-phase boundaries (B).

the lower density phase (hexacelsian). The transformation of the hexacelsian phase to its anorthite polymorph occurred at higher crystallization temperatures were deformation of the glass allowed the associated stresses to be relieved. Similarly, the first titania phase to form in these glass–ceramics was anatase ($3.89\,g\,cm^{-3}$), which was followed by the formation of rutile ($4.25\,g\,cm^{-3}$). These structural phenomena were observed over a wide range of $SrO–TiO_2–SiO_2–Al_2O_3$ compositions and crystallization conditions [9].

At low crystallization temperatures (850 and 900° C), the formation of $SrTiO_3$ resulted in a spherulitic growth texture, in which dendrites radiated from nucleation sites. These textures are typical of glass–ceramics prepared under conditions in which the nucleation and growth of crystalline phases are difficult [14–15]. This type of microstructure was also observed in glass–ceramics of the analogous $PbO–TiO_2–SiO_2–Al_2O_3$ system [5]. The fine structural spot splitting, observed by SAED, was likely caused by tilt-boundaries as the $SrTiO_3$ crystals grew. As the crystallization temperature (or time) was increased, interstitial growth of hexacelsian $SrAl_2Si_2O_8$ inhibited the further growth of $SrTiO_3$, as evidenced by the TEM observation of interrupted dendritic growth. The growth of the hexacelsian phase mainly inhibited the growth of the secondary branches (nodes) of the dendritic crystals of $SrTiO_3$. In glass–ceramics crystallized at 1000° C, the interstitial crystallization of the hexacelsian phase was rapid enough to prevent the dendritic growth of $SrTiO_3$, resulting in dispersed $SrTiO_3$ crystals. As the crystallization temperature was increased to 1100° C, the morphology of the $SrTiO_3$ crystals changed dramatically; the $SrTiO_3$ crystals were much larger and faceted. This indicates that the nucleation and growth kinetics were much improved at this temperature.

The presence of large acicular rutile crystals was the dominant microstructural feature in glass–ceramic samples crystallized for longer times at 1100° C. This is an apparent contradiction with XRD data, which suggested that the rutile was only a minor phase in these glass–ceramics. The crystallographic shear planes (CSP) and anti-phase boundaries, observed within the rutile crystals, were similar to microstructural features in rutile crystals as reported by other workers [16–17]. Rapid growth of the rutile crystals may have made it difficult for the crystals to maintain stoichiometry, and the CSP may have formed to accommodate non-stoichiometric regions within the rutile crystals by edge sharing of octahedra.

5. Conclusions

In this $SrO–TiO_2–SiO_2–Al_2O_3$ glass–ceramic system, the crystalline phases observed and the final microstructures were strongly dependent on the crystallization conditions, and the following observations were made.

(1) At low crystallization temperatures (800 to 900° C), the initial crystallization of perovskite $SrTiO_3$ occurred via a spherulitic crystal growth mechanism, resulting in dendritic $SrTiO_3$ crystal clusters, composed of 20 nm crystallites. As the crystallization time was increased, hexacelsian $SrAl_2Si_2O_8$ crystallized interstitially, interrupting the dendritic growth of the $SrTiO_3$.

(2) At higher temperatures (900 to 1000° C), a competition for strontium occurred between the $SrTiO_3$ and $SrAl_2Si_2O_8$ hexacelsian phases. The microstructure consisted of dispersed $SrTiO_3$ crystallites (50 nm) and larger (200 nm) hexacelsian crystals.

(3) At a crystallization temperature of 1100° C, the morphology of the $SrTiO_3$ phase consisted of larger (500 nm) faceted crystals, and hexacelsian $SrAl_2Si_2O_8$ transformed gradually with time to its anorthite polymorph. Also at 1100° C, titania crystallized, first as small (300 nm) crystals, and then as large acicular rutile crystals which grew to 80 μm in length after 16 h.

Acknowledgements

Financial support for this work was provided by the US Army Research Office under Contract No. DAAG-82-K-0015. The authors would like to thank Tooser Wilson and Beth Jones (Materials Research Laboratory, Pennsylvania State University) for assistance in the experimental aspects of this research, along with A. S. Bhalla and L. E. Cross (Materials Research Laboratory, Pennsylvania State University), W. N. Lawless (CeramPhysics, Inc., Westerville, Ohio) and C. M. O. Alexander (Department of Physics, University of Essex) for helpful discussions.

References

1. A. HERCZOG, *J. Amer. Ceram. Soc.* **47** (1964) 107.
2. T. KOKUBO, C. KUNG and M. TASHIRO *J. Ceram. Assoc. Jpn* **76** (1968) 128.
3. D. HULSENBERG and J. LEHMAN, *Silakattechnik* **34** (1983) 74.
4. T. KOKUBO and M. TASHIRO, *J. Non-Cryst. Solids* **13** (1973/1974) 328.
5. M. A. G. C. van de GRAAF, J. C. LODDER and A. J. BURGRAAF, *Glass Tech.* **15** (1974) 143.
6. S. M. LYNCH and J. E. SHELBY, *J. Amer. Ceram. Soc.* **67** (1984) 424.
7. W. N. LAWLESS, *Ferroelectrics* **3** (1972) 287.
8. *Idem, ibid.* **7** (1974) 379.
9. S. L. SWARTZ, PhD Thesis, The Pennsylvania State University (1985).
10. W. N. LAWLESS, Private communication.
11. W. N. LAWLESS and B. WEDDING, *J. Appl. Phys.* **41** (1970) 1926.
12. H. P. KLUG and L. E. ALEXANDER, in "X-ray Diffraction Procedures", John Wiley, New York (1954) p. 491.
13. J. TOPEL-SCHADT, W. F. MULLER and H. PENTINGHAUS, *J. Mater. Sci.* **13** (1978) 1809–1816.
14. H. D. KEITH and F. J. PADDEN, *J. Appl. Phys.* **34** (1963) 2409.
15. S. W. FREIMAN, G. Y. ONADA and A. G. PINCUS, in "Advances in Nucleation and Crystallization in Glass" (edited by L. L. Hench and S. W. Freiman) The American Ceramic Society, Columbus, Ohio (1971) p. 141.
16. S. S. SHINOZAKI, W. T. DONION and A. H. MEITZLER, *J. Appl. Phys.* **53** (1982) 7290.
17. L. C. OTERO-DIAZ, J. SORIA and M. A. ALARIO-FRANCO, *Phys. Status Solidi* **82** (1984) 379.

Received 23 September 1987
and accepted 26 January 1988